

Absolute X-ray energy measurement using a high-accuracy angle encoder

Takahiko Masuda,^{a,*} Tsukasa Watanabe,^{b,†} Kjeld Beeks,^c Hiroyuki Fujimoto,^b Takahiro Hiraki,^a Hiroyuki Kaino,^a Shinji Kitao,^d Yuki Miyamoto,^a Koichi Okai,^a Noboru Sasao,^a Makoto Seto,^d Thorsten Schumm,^c Yudai Shigekawa,^e Kenji Tamasaku,^f Satoshi Uetake,^a Atsushi Yamaguchi,^e Yoshitaka Yoda,^g Akihiro Yoshimi^a and Koji Yoshimura^a

Received 16 April 2020

Accepted 2 November 2020

Edited by A. Bergamaschi, Paul Scherrer Institut, Switzerland

† These authors contributed equally to this work.

Keywords: X-ray diffraction; energy calibration; lattice constants; rotary encoders; nuclear resonant scattering.

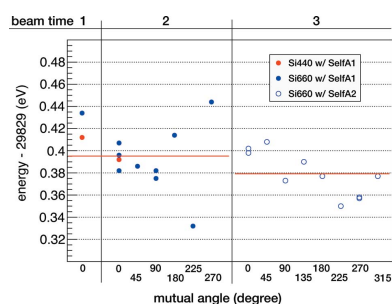
^aResearch Institute for Interdisciplinary Science, Okayama University, Okayama, Japan, ^bNational Institute of Advanced Industrial Science and Technology, Tsukuba, Japan, ^cInstitute for Atomic and Subatomic Physics – Atominstut, TU Wien, Vienna, Austria, ^dInstitute for Integrated Radiation and Nuclear Science, Kyoto University, Kumatori-cho, Japan, ^eRIKEN, Wako, Japan, ^fRIKEN, SPring-8 Center, Sayo-cho, Japan, and ^gJapan Synchrotron Radiation Research Institute, Sayo-cho, Japan. *Correspondence e-mail: masuda@okayama-u.ac.jp

This paper presents an absolute X-ray photon energy measurement method that uses a Bond diffractometer. The proposed system enables the prompt and rapid *in situ* measurement of photon energies over a wide energy range. The diffractometer uses a reference silicon single-crystal plate and a highly accurate angle encoder called SelfA. The performance of the system is evaluated by repeatedly measuring the energy of the first excited state of the potassium-40 nuclide. The excitation energy is determined as 29829.39 (6) eV, and this is one order of magnitude more accurate than the previous measurement. The estimated uncertainty of the photon energy measurement was 0.7 p.p.m. as a standard deviation and the maximum observed deviation was 2 p.p.m.

1. Introduction

A synchrotron radiation X-ray beam is often monochromated by silicon monochromators installed on the beamline. The energy bandwidth of this monochromated beam is usually a few electron volts (eV), and a narrower than sub-eV bandwidth is also easily available by using high-resolution monochromators. A monochromatic beam is used in various research fields that require an accurate photon energy. For example, in nuclear resonant scattering (NRS) experiments (Seto, 2012), narrow resonance peaks of NRS sometimes need to be found. Knowing the accurate photon energy helps in finding the resonance without wide energy scanning, which is especially useful when searching for weak resonance peaks. Accurate photon energy information is also needed to determine the lattice spacing of samples for the structural determination of crystalline, non-crystalline and nano-materials (Billinge & Levin, 2007).

While various absolute energy calibration methods have been proposed thus far (Arthur, 1989; Kraft *et al.*, 1996; Hong *et al.*, 2012), the most commonly used technique is to measure the absorption edge of a reference element. Although the absolute photon energy is adjusted at a certain absorption edge, the absolute photon energy easily deviates over time because of uncontrollable factors, such as a change in the thermal distribution of the monochromators. In particular, in NRS measurements, the photon energy is scanned to search for a resonance peak; the scanning operation changes the



monochromator condition and energy drifts are unavoidable. The absorption-edge measurement method cannot overcome such problems. Therefore, an easily available *in situ* method that can calibrate the absolute photon energy over a wide energy range would be highly appreciated.

The authors recently demonstrated an NRS measurement of the thorium-229 nucleus (Masuda *et al.*, 2019b) to study its low-energy first excited state, called an isomer (Thielking *et al.*, 2018; Burke, 2019; Seiferle *et al.*, 2019). In that work, the thorium nuclei were resonantly excited to the second nuclear state by irradiating them with a monochromatic X-ray beam. Accurate X-ray photon energy measurement was a key component of the work. Since the resonance is weak and there is a large non-resonant scattering background, the X-ray photon energy had to be sufficiently monochromated and stabilized over a long period. More specifically, the resonance energy was 29 keV, and the bandwidth of the X-ray photon energy was ~ 0.1 eV; therefore, the photon energy had to be monitored at a 1 p.p.m. level during 24 hour scanning. Further, the absolute energy can be used to determine the isomer energy accurately by combining with high-accuracy γ -ray spectroscopies (Yamaguchi *et al.*, 2019).

The absolute energy measurement system used in the present study utilizes a method developed by Bond (1960), which was originally used for crystal lattice-spacing measurements. This method is based on Bragg's law: the relation between the wavelength of an X-ray photon λ_{Xray} , which is the inverse of the photon energy E_{Xray} , and the crystal lattice spacing d is $\lambda_{\text{Xray}} = 2d \sin \theta_{\text{B}}$, where θ_{B} is the Bragg angle of the crystal. To increase the measurement accuracy, Bond proposed and designed a measurement scheme in which the X-ray Laue diffraction angle of a reference crystal is measured on both sides of the primary beam. This method can eliminate zero-point offset because it uses the angle difference between the two diffractions. It can also eliminate possible setting errors of the crystal by *in situ* alignment. The Bond method has been widely used for the lattice-spacing determination of various crystals, and the reported uncertainties are $\Delta d/d \simeq 10^{-5}$ (Herbstein, 2000; Schmidbauer *et al.*, 2012).

For X-ray photon energy calibration, the Bragg angle is measured with a reference crystal whose lattice spacing is well known. The lattice spacing of a silicon single crystal has been well established with an accuracy of $\Delta d/d \simeq 10^{-7}$ (Cavagnero *et al.*, 2004a,b). Therefore, the key to an accurate absolute energy measurement is the accurate measurement of the diffraction angle. For example, the accurate energy calibration of X-ray absorption edges of the order of 10^{-5} to 10^{-6} has been reported using a silicon reference crystal and a Bond diffractometer (Kraft *et al.*, 1996); the angle uncertainty was ± 0.12 arcsecond measured by a dedicated calibration method (Becker & Stümpel, 1990).

In the present study, we used a rotary encoder equipped with a self-calibration function, called SelfA (Watanabe *et al.*, 2005), for accurate angle measurement. It was originally developed at the National Metrology Institute of Japan and is now commercially available. The accuracy of the angle measurement is better than 0.1 arcsecond.

In this study, we adapted an accurate rotary encoder based on SelfA for a Bond diffractometer to the absolute photon energy measurement of a synchrotron radiation X-ray beam. This method can perform *in situ* measurements within ~ 3 min and it can be applied to any energy range. The apparatus can be easily positioned at the downstream end of an experiment such that the main experiment is not disturbed. We took repeated measurements of the excitation energy of the first excited state of the potassium-40 (^{40}K) nucleus with various settings to verify the reliability of this method.

2. Bond diffractometer

2.1. Principle

The Bond diffractometer measures the absolute energy of X-ray photons based on the Bragg diffraction angle (θ_{B}) from a silicon single-crystal plate (Si plate). The accurate relation between the X-ray photon energy E_{Xray} and the diffraction angle is

$$E_{\text{Xray}} = \frac{1.239841857 \text{ (keV nm)}}{2d(P, T) \sin \theta_{\text{B}} \sin \theta_{\text{beam}} \sin \theta_{\text{recip}}}, \quad (1)$$

$$d(P, T) = \frac{d_{220}}{2} \left(1 - \frac{PC_{\text{comp}}}{3} \right) \times \left\{ 1 + [T - 22.5 \text{ (}^\circ\text{C)}] C_{\text{temp}} \right\}, \quad (2)$$

where P and T are the ambient pressure and temperature, respectively, θ_{beam} is the angle between the Si plate rotation axis and the primary beam, and θ_{recip} is the angle between the Si plate rotation axis and the reciprocal-lattice vector of the crystal. These angles are shown graphically in Fig. 1(a). The numerator of equation (1) is the conversion factor of the wavelength to the energy of the X-ray photons. The lattice spacing d depends on the temperature and pressure as described in equation (2). The parameter d_{220} is the lattice spacing of the (220) lattice planes at $T = 22.5^\circ\text{C}$ and in a vacuum ($P = 0$ Pa), C_{temp} is a thermal expansion coefficient and C_{comp} is the compressibility. The first 1/2 factor is added because we used the (440) lattice planes. The Si plate rotation axis has to be perpendicular to both the primary beam and the reciprocal-lattice vector of the crystal so that $\theta_{\text{beam}} = \theta_{\text{recip}} = 90^\circ$ is satisfied. Deviations of these angles cause systematic uncertainty; their accuracy is not crucial, however, for their first derivatives are zero.

2.2. SelfA

The diffraction angle is measured by a rotary encoder controlled with SelfA. SelfA utilizes the equal division averaged method (Masuda & Kajitani, 1993) that relies on the fact that the angle is a 360° closed system. It analyzes the angular deviation by evaluating angular signals from multiple reading heads located at equal angular intervals around the grating lines on a rotary disk. The reading heads sense the grating lines that pass over the heads during a rotation. The signal detected from the grating lines contains the angular deviation from the ideal angular signal.

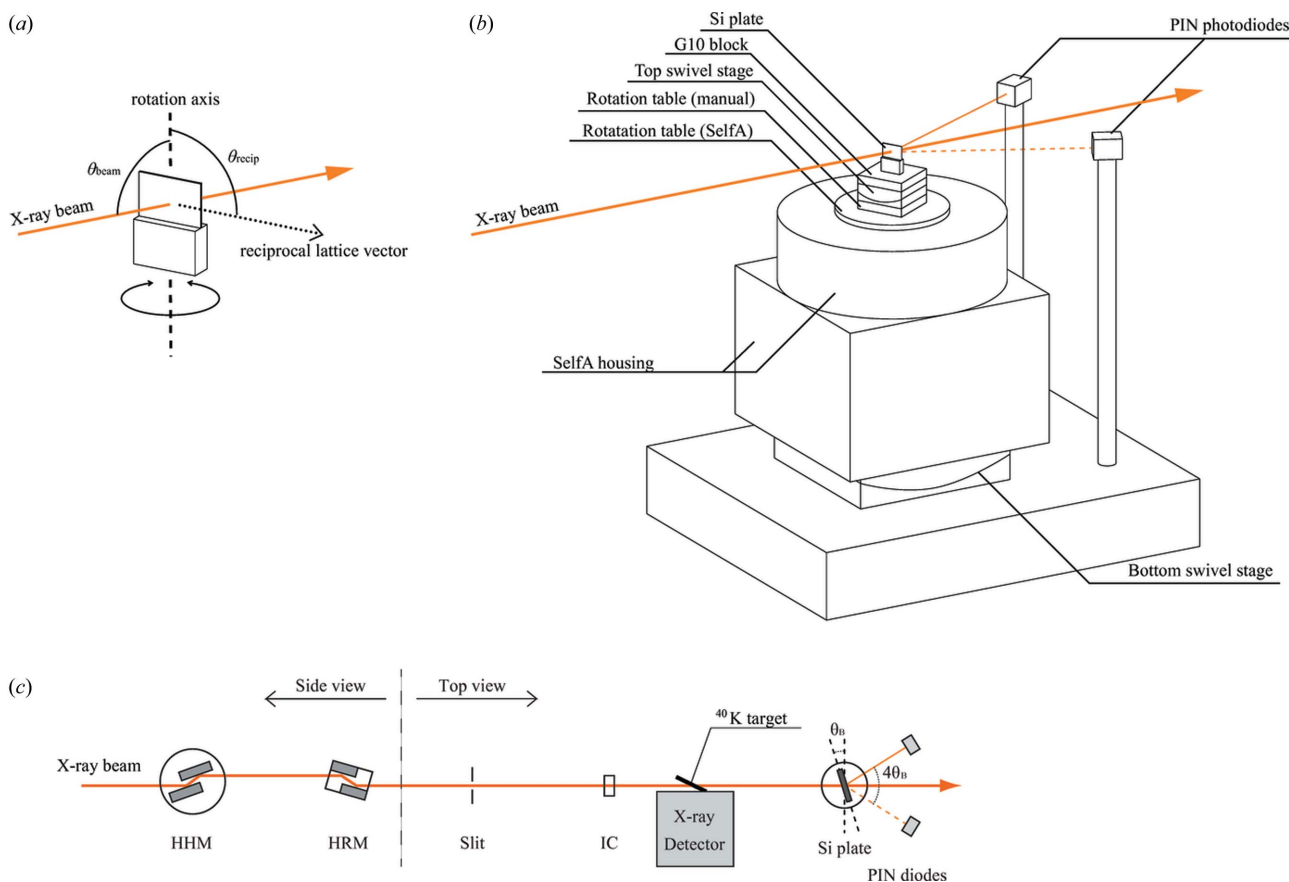


Figure 1

(a) A schematic diagram of the Si plate. The geometric arrangement of the X-ray primary beam, the plate rotation axis and the reciprocal-lattice vector of the crystal is drawn. (b) A schematic diagram of the Bond diffractometer. (c) A schematic diagram of the beamline. HHM is the high heat-load monochromator, HRM is the high-resolution monochromator, IC is the ionization chamber and θ_B the Bragg angle. The X-ray beam, shown as the orange lines, comes in from the left-hand side and passes through the Si plate in each panel. The diffracted beams are indicated by thin orange lines. In panels (b) and (c), the Si plate is rotated by the Bragg angle from the angle perpendicular to the beam, and one PIN photodiode receives the diffracted beam.

If N reading heads are arranged at $360^\circ/N$ intervals, the system can detect the angular deviation except for the $n \times N$ th order Fourier components (n is an integer); therefore, the number of reading heads should be large to ensure accurate calibration (Watanabe *et al.*, 2014). Although a larger N is required to improve calibration, which enables one to detect higher-order Fourier components, the higher-order components have less effect on the angle deviation than the lower-order components. Moreover, if another M reading heads are arranged at $360^\circ/M$ intervals with the original N reading heads, some $n \times N$ th order Fourier components can be obtained, and the remaining undetected Fourier components are only $n \times N \times M$ th order Fourier components. Therefore, a setup with N reading heads arranged at $360^\circ/N$ intervals and M reading heads arranged at $360^\circ/M$ intervals is equivalent to $N \times M$ reading heads arranged at $360^\circ/(N \times M)$ intervals.

In this work, we used SelfA, which has 12 reading heads, and these heads were placed at $1/3$ (120°), $1/4$ (90°) and $1/7$ (51.43°) positions around a rotary disk, as shown in Fig. 2. This setup can be used to detect the angular deviation from the ideal exact equally spaced lines, except for the $84n$ th order Fourier components.

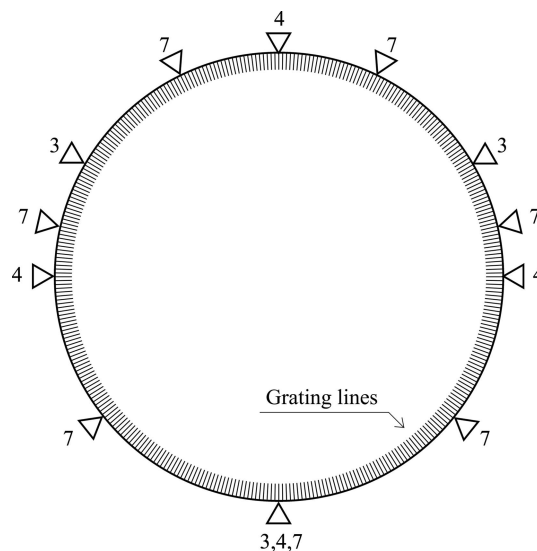


Figure 2

A schematic diagram of the rotary encoder equipped in SelfA. The 12 triangles represent the reading heads and their labels indicate their grouping.

The rotary encoder has 36000 grating lines with an angular pitch of 0.01° . These signals read by the heads are electrically divided into 1024 subpoints by an interpolating circuit between the grating pitches to increase the angular granularity to 36000×1024 , which corresponds to the angular pitch of 0.03515625 arcsecond.

2.3. Instruments

The Bond diffractometer comprises a rotation table based on SelfA, a manual rotation table, a Si plate, two motorized swivel stages and two silicon PIN photodiodes. A schematic diagram is shown in Fig. 1(b), and a photograph is shown in Fig. 3.

The Si plate was placed at the top of the apparatus. The Si plate (0.5 mm thick) was cut from the same ingot of the standard reference crystal as used in a previous study (Cavagnero *et al.*, 2004a,b) with natural isotopic compositions; in that study, the lattice spacing d_{220} of the (220) lattice planes was measured carefully. The Si plate was glued onto an aluminium plate and covered with an aluminium cover (not shown in Figs. 1 and 3), which had polyimide beam windows at both ends. It was also covered with foamed polystyrene to stabilize the temperature around the Si plate. A glass epoxy G10 block was inserted between the crystal and the motorized components at the bottom for thermal isolation. Two temperature sensors, calibrated to an absolute accuracy of greater than $\Delta T = \pm 5$ mK in advance, were set inside the

aluminium cover. The sensors were read by a thermometer readout module (Fluke Black Stack Thermometer 1560 and Platinum Resistance Thermometer Scanner 2562) with an absolute accuracy of $\Delta T = \pm 10$ mK.

The Si plate was mounted on a stack consisting of a top motorized swivel stage, a manual rotation table, a rotation table based on SelfA and a bottom motorized swivel stage, from top to bottom. The two swivel stages were used to align the mutual angles along the three axes. The manual rotation table was used to check the uniformity of SelfA; the details are described in Section 3.2.

The rotation table based on SelfA was manufactured by e-motion system Inc. All the electronics were housed in the bottom case. The rotation table was supported by an air bearing.

The two silicon PIN photodiodes were used for detecting the diffracted beam. These photodiodes were placed such that the angle difference between the primary beam and the line from the Si plate to a photodiode was twice the Bragg angle. The sensitive area of the photodiodes was 28×28 mm and the thickness was 500 μm . These were disposed at an angle of $\sim 45^\circ$ to the incident beam. The output current from the photodiodes was read out by current amplifiers (Keithley 428).

2.4. Measurement procedure

For absolute energy measurement, the X-ray beam diffractions were monitored while rotating the Si plate. X-ray diffraction occurred only when the angle between the primary beam and the reciprocal-lattice vector of the crystal coincided with the Bragg angle. Fig. 4 shows the diffraction peak monitored by one PIN photodiode. We rotated the rotary encoder by ~ 0.4 arcsecond and fixed it each time. We repeated this 0.4 arcsecond rotation step 100 times as shown in the figure. It took ~ 1 s for a step. The rotation angle at the diffraction center on each side of the primary beam was obtained by fitting with a Gaussian function. The angle

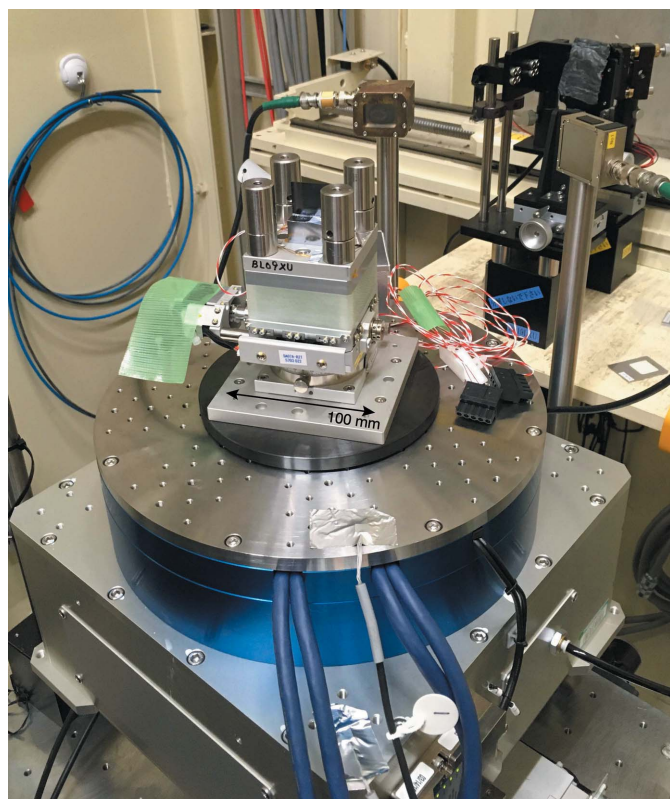


Figure 3
A photograph of the Bond diffractometer. The black circular plate is the rotation table based on SelfA.

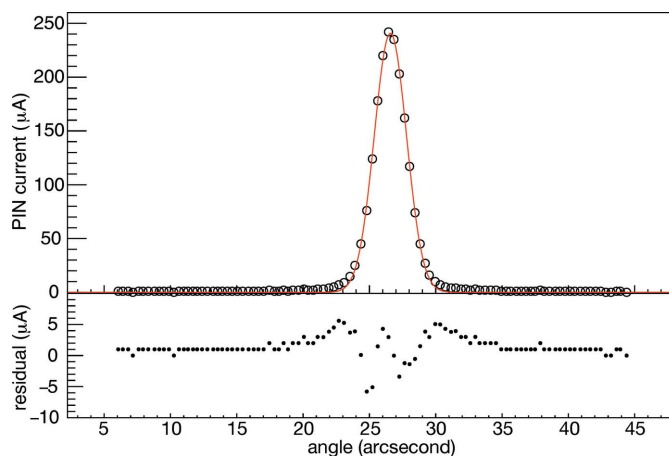


Figure 4
(Top) The X-ray diffraction peak measured on one side. The horizontal axis is the Si plate rotation angle controlled by SelfA, and the vertical axis is the output current from the PIN photodiode. (Bottom) The residual plot of the upper figure.

Table 1
Parameters of NRS measurements.

Beam time	Bunch mode	HRM	SelfA
1	A	Si(440), Si(660)	1
2	A	Si(440), Si(660)	1
3	D	Si(660)	2

difference between the two peaks $\Delta\theta$ was $2\theta_B$. Finally, the X-ray photon energy was determined by substituting the obtained θ_B into equation (1).

Before the actual photon energy measurement, the two swivel stages should be adjusted. For this, we measured and minimized the angle difference $\Delta\theta$ by rotating the swivel stages. We iterated the adjustment of the swivel stages individually. Next, we disconnected the power cable of the upper swivel stage and performed the self-calibration of SelfA. Since 360° rotation is required for SelfA calibration, the temperature sensor cables were also disconnected to prevent tangling.

3. Measurement

3.1. NRS measurement

We performed the NRS measurements at SPring-8 on the BL19LXU beamline (Yabashi *et al.*, 2001). We measured the resonance energy of the first excited state of the ^{40}K nuclide, with a resonance energy and half-life of $E_{\text{res}} = 29829.9$ (6) eV (Firestone, 1999) and 4.24 (9) ns (Endt, 1990), respectively. Its energy linewidth is sufficiently narrow compared with the energy bandwidth of the X-ray beam and can be ignored; thus, this excited state is a good target for NRS measurement. We carried out the measurements in three beam times with two units of SelfA to verify reproducibility. The parameters are listed in Table 1.

In beam times 1 and 2, the bunch mode was A, in which 203 identical electron bunches were equally spaced with a time interval of 23.6 ns in the storage ring. In beam time 3, the bunch mode was D, in which 15% of the total current was shared in five bunches with a time interval of 684.3 ns, and the remaining 85% was shared equally in successive bunch trains in 1/7 of the circumference with a repetition rate of 1.966 ns (SPring-8, 2020).

For the SelfA units, the first one, which was used for beam times 1 and 2, was manufactured in 2007, and the second one, which was used for beam time 3, was manufactured in 2019. Other parts such as the Si plate, temperature sensors and swivel stages were identical for all beam times.

The experimental overview is shown in Fig. 1(c). The X-ray beam was monochromated by two silicon monochromators. The first Si(111) monochromator was a high heat-load monochromator (HHM). After passing through the HHM, the intensity was 8×10^{13} photons s^{-1} and the energy bandwidth was 3.4 eV FWHM. The second monochromator was a high energy-resolution monochromator (HRM); we used Si(440) or Si(660) as the HRM. The beam size was defined to be approximately 0.4×0.4 mm by the slit located after the

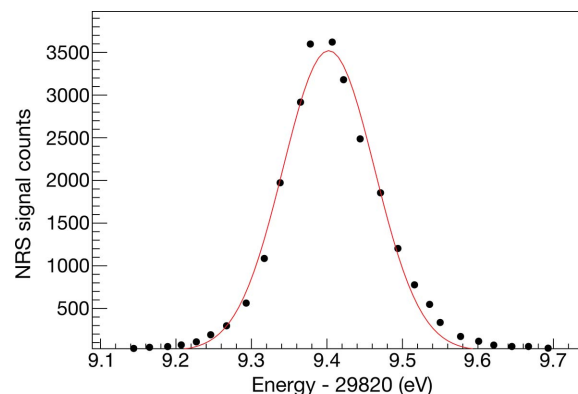


Figure 5
The resonance curve of the first excited state of ^{40}K .

HRM. The beam intensity was 4×10^{12} (1×10^{12}) photons s^{-1} and the FWHM of the energy bandwidth was 0.26 eV for Si(440) [0.10 eV for Si(660)]. The beam intensity was monitored using an ionization chamber positioned after the slit. The monochromated beam passed through the ^{40}K target and then through the Bond diffractometer at the downstream end.

The apparatus of the NRS measurement was almost identical to that used in previous work (Yoshimi *et al.*, 2018; Masuda *et al.*, 2019b), only the target was different. The ^{40}K target was a KCl pellet (diameter 3 mm, thickness 0.5 mm) prepared by pressing 5 mg KCl powder with ~ 2 MPa. Because the natural abundance of ^{40}K is only 0.01%, we used 4% enriched potassium. The pellet was covered with two 20×20 mm MgF_2 substrates, one on either side. The scattered X-ray photons were detected by a dedicated energy-sensitive X-ray detector (Masuda *et al.*, 2017, 2019a).

For the NRS measurements, the HRM was tuned to scan the photon energy. A typical resonance curve is shown in Fig. 5. We repeated the following procedure to obtain one resonance curve: rotate the HRM, measure the absolute energy of the photons, then accumulate the NRS data for 100 s. One point of a resonance curve was obtained in 4–5 min. The resonance energy was obtained by fitting the resonance curve with a Gaussian function, as shown in Fig. 5. The data points deviate slightly from the fitting function but no regular deviation pattern was found. The deviation could be caused by photon energy fluctuation or drifts over time because we took the data directly after rotating the HRM.

3.2. Reproducibility and uniformity

To verify the reproducibility and uniformity of the system, we performed NRS measurements for various mutual angles between the Si plate and the rotation table based on SelfA by rotating the manual rotation table between these. For beam times 2 and 3, the resonance peaks were measured with six and eight angle settings, respectively, as shown in Fig. 6. We performed swivel adjustment and self-calibration functions after every rotation of the manual rotation table. The unit of SelfA for beam times 1 and 2 was different from that for beam

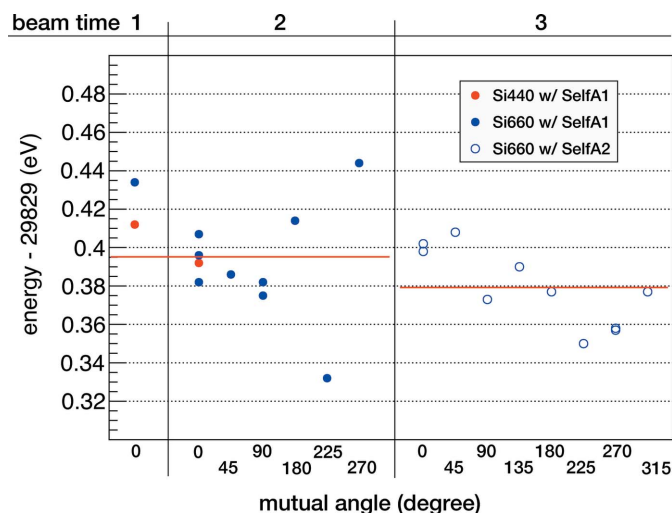


Figure 6 Resonance peak values of each ⁴⁰K NRS measurement. The numbers along the top indicate the beam time, and those at the bottom are the mutual angles between the Si plate and the rotation table. The horizontal red bars are the averaged values of the measurements with SelfA1 or SelfA2.

time 3; therefore, the mean value of the resonance energy was evaluated for each unit of SelfA. We found that the mean values of the resonance energy were consistent within $\Delta E_{\text{res}} = 0.02$ eV ($\Delta E_{\text{res}}/E_{\text{res}} = 0.7$ p.p.m.) between the SelfA units, while the maximum deviation from the average was $\Delta E_{\text{res}} = 0.06$ eV ($\Delta E_{\text{res}}/E_{\text{res}} = 2.0$ p.p.m.). This demonstrates the reproducibility, including the individual differences between SelfA units and beam times.

3.3. Uncertainty analysis

3.3.1. Lattice spacing of the silicon crystal. We quote the lattice spacing as $d_{220} = 192.01559$ (2) pm, considering the inhomogeneity of the crystal (Cavagnero *et al.*, 2004a,b). The energy uncertainty due to this inhomogeneity was 0.10 p.p.m.

For the thermal expansion effect, the uncertainties in the temperature and thermal expansion coefficient were considered. The difference between the two temperature sensors was ~ 0.026 K. This difference can be considered as the temperature gradient inside the cover that arises because of the heat load from the lower motorized components. We considered half of the difference (0.013 K) as the uncertainty. A local temperature deviation inside the Si plate where it was actually irradiated by the X-ray beam will cause uncertainty. The heat load of the Si plate due to the X-ray beam was estimated as ~ 0.5 mW. We estimated that the local temperature increase at the irradiation spot was lower than 0.01 K through a finite-element analysis calculation. The thermal expansion coefficient we used was $C_{\text{temp}} = 260.00 \times 10^{-8} \text{ K}^{-1}$ based on a previous study (Lyon *et al.*, 1977). Although the coefficient depends slightly on temperature, it is sufficient to use a constant value because the average between the base temperature (22.5°C) and the actual temperature (27.5°C) is $C_{\text{temp}} = 260.11 \times 10^{-8} \text{ K}^{-1}$. Therefore, the temperature dependence of the coefficient was not taken into account.

Table 2 Uncertainty related to lattice spacing d .

Parameter	Value	Uncertainty	Contribution (p.p.m.)
Lattice spacing d_{220}	192.01559 pm	0.00002 pm	0.10
Temperature monitor T	$\sim 27.5^\circ\text{C}$	0.013 K	0.03
Local heating T		0.009 K	0.02
Temperature expansion coefficient C_{temp}	$260.00 \times 10^{-8} \text{ K}^{-1}$	$0.11 \times 10^{-8} \text{ K}^{-1}$	<0.01
Total			0.11

For compression due to ambient pressure, we did not correct the pressure effect or use a pressure sensor in this study. Even though the uncertainty in the pressure is $\Delta P/P = 10\%$, the uncertainty in the energy is less than 0.05 p.p.m. because the compressibility is only $C_{\text{comp}} = 1.0221$ (3) $\times 10^{-11} \text{ Pa}^{-1}$ (Hall, 1967); therefore, the compression effect was ignored in this study.

By summing the uncertainties mentioned above in quadrature, the uncertainty due to the lattice spacing was estimated to be $\Delta d/d = 0.11$ p.p.m. These uncertainties and their contributions to the lattice spacing are summarized in Table 2.

3.3.2. SelfA angle measurement. The uncertainty in the angle measurement by SelfA was classified into four parts.

The rotary encoder was servo-controlled with a resolution of 0.035 arcsecond per pulse. A quantization uncertainty of $0.035/2\sqrt{3}$ arcsecond $\simeq \pm 0.010$ arcsecond should be considered.

While the crystal angle was fixed, the angle deviated for one pulse. Therefore, the maximum angle deviation should be less than 1 ± 1 pulses, and a quantization uncertainty in a rectangular distribution with a width of 3 pulses [$0.035 \times 3/2\sqrt{3}$ arcsecond = ± 0.030 arcsecond] was added to the uncertainty.

The calibration values of SelfA could fluctuate at a certain level because of the variation in the measuring environment. To estimate the fluctuation, we performed three calibrations for each calibration sequence and used the averaged values of these three cycles. Fig. 7 shows the individual calibration values for the three cycles along with their average. Note that the figure is an enlarged view that shows only the 0.02° region from the entire 360° circumference. Fig. 8 shows the averaged calibration values for the entire circumference. We evaluated the standard deviation from the average to be less than ± 0.030 arcsecond.

The last factor was the higher-order Fourier components that SelfA cannot detect. A detailed explanation of this analysis procedure is provided in a previous report (Watanabe *et al.*, 2014). As mentioned in Section 2.2, the self-calibration function cannot detect the 84th order Fourier components. This magnitude can be estimated from the lower-order components. Figs. 9 and 10 show the typical discrete Fourier transformed (DFT) components of the calibration values. According to Fig. 9, any components higher than the 18th order are less than 0.01 arcsecond; thus, the 84th order

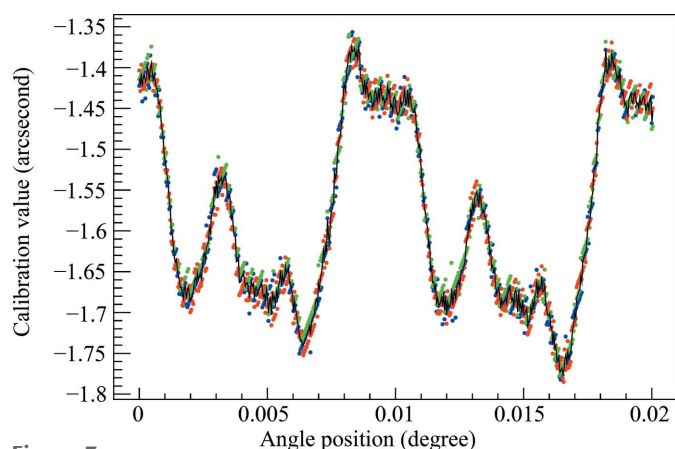


Figure 7
Calibration values obtained by performing the self-calibration function three times. The horizontal axis shows the rotation angle of the SelfA unit calculated based on the number of steps of the rotary encoder, and the vertical axis is the calibration value for each rotation angle. The colored points are individual calibration values; each color represents a different calibration sequence. The black line is the average of the three sequences.

components could be assumed to be lower than 0.01 arcsecond as well.

The peak components in Fig. 10 are due to electrical interpolation, which appeared every 36000 components. The $7n$ -th order components of the interpolation (252000th) cannot be detected and these can also be assumed to be less than 0.01 arcsecond.

By summing the uncertainties listed in this subsection in quadrature, the angle uncertainty due to the SelfA unit was estimated to be 0.044 arcsecond and the corresponding photon energy uncertainty was $\Delta E_{X\text{ray}}/E_{X\text{ray}} = 0.67$ p.p.m. This was the dominant uncertainty in our estimations. These uncertainties in the angle measurement are listed in Table 3.

3.3.3. Other sources. The effects due to the uncertainty of the swivel setting were estimated from the repeatability of the angle measurement of the swivels. The repeatability was conservatively $\Delta\theta_{\text{beam}} = \Delta\theta_{\text{recip}} = 0.01^\circ$ and the corresponding photon energy uncertainty was 0.03 p.p.m. Because the diffraction peak shapes (shown in Fig. 4) are dominated by the

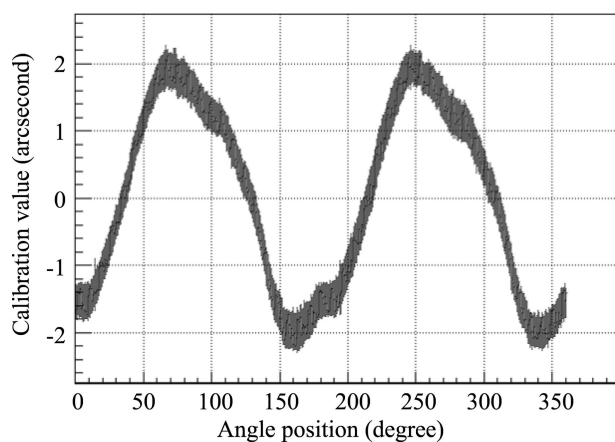


Figure 8
The averaged calibration value for each angle position along the entire circumference of the rotary encoder.

Table 3
Uncertainty related to angle measurement.

Parameter	Value	Angle uncertainty
Angle quantization	0.035 arcsecond	0.010 arcsecond
Servo-control quantization	0.105 arcsecond	0.030 arcsecond
Calibration fluctuation		0.030 arcsecond
Higher-order Fourier components		<0.01 arcsecond
Total		0.044 arcsecond

horizontal angular divergence of the incident beam, the shapes on both sides are supposed to be identical; therefore, the difference between these sides should be considered as the systematic uncertainty. We estimated this effect by fitting the shapes to various functions as well as to a simple Gaussian function, and we conservatively adopted the maximum deviated function. The resulting uncertainty was 0.0083 arcsecond for θ_B ; the corresponding photon energy uncertainty was 0.17 p.p.m. The statistical precision of the diffraction peak center determination by the Gaussian fit was estimated as 0.0095 arcsecond for a diffraction peak. The corresponding photon energy uncertainty was 0.14 p.p.m. The last uncertainty is categorized as a random error, while the other uncertainties are systematic for the X-ray photon energy

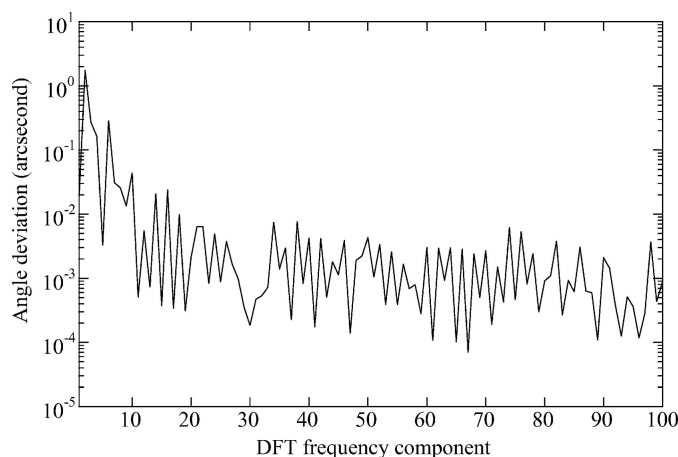


Figure 9
The DFT component below the 100th order.

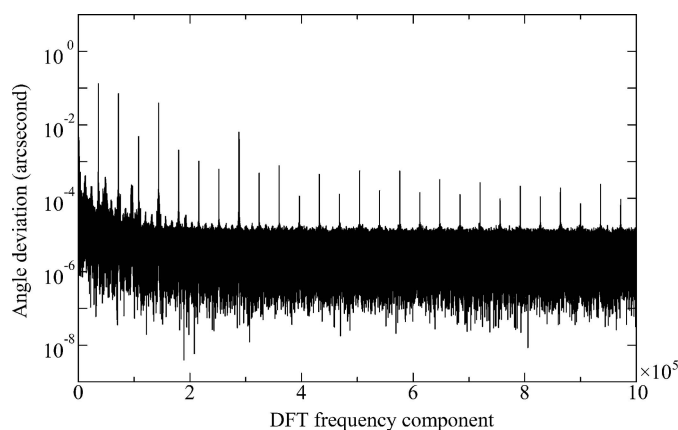


Figure 10
The DFT component up to the 1×10^6 th order.

Table 4
Energy uncertainty estimation list.

Parameter	Contribution (p.p.m.)
Lattice spacing	0.11
Angle measurement by SelfA	0.67
Diffraction center determination (random)	0.14
Diffraction peak shape	0.17
Swivel setting	0.03

measurement because it is reasonable to suppose that the swivels setting and the beam angle divergence are unchanged during measurements.

In addition, we checked the dependence of the rotation direction on the rotation table and beam intensity, which were not supposed to affect the measurements. The change in the measured resonance energy was 0.23 p.p.m. when the rotation direction was reversed. For the beam intensity effect, we reduced the beam intensity by half, and the measured resonance energy was stable within 0.04 p.p.m. from the original intensity. Since these two effects were smaller than the estimated uncertainty, they can be ignored.

3.4. Results

Among the NRS measurements for the three beam times, the maximum deviation from the average of the measured resonance energy was observed at a level of 2 p.p.m., while the estimated uncertainty of the photon energy measurement, which we have discussed in this section, was 0.7 p.p.m. as a standard deviation in total. Table 4 summarizes the uncertainties discussed in this section.

We determined the excitation energy by averaging all the values, and we conservatively quote the maximum deviation as the uncertainty: 29829.39 ± 0.06 eV. This result is one order of magnitude better than the previously reported value of 29829.9 ± 0.6 eV (Firestone, 1999).

4. Conclusions

We have reported a new absolute X-ray energy measurement method. The method uses a Bond diffractometer with a silicon single-crystal plate and a commercially available rotation table. We have measured the resonance energy of the first excited state of the ^{40}K nuclide via the NRS technique and demonstrated the performance of the proposed method. The results, which were obtained using two different units of SelfA, show good agreement, better than $\Delta E/E = 0.7$ p.p.m. While the estimated uncertainty in the photon energy measurement is at a level of 0.7 p.p.m., the observed reproducibility was found to be 2 p.p.m. at the maximum deviation from the average. We have improved the energy measurement of the first excited nuclear state of the ^{40}K nuclide by one order of magnitude. This improvement is achieved based primarily on the high-accuracy angle encoder, SelfA, which is able to determine the rotation angle with an accuracy of the order of 0.1 arcsecond. The system can be applied to a wide energy range of the X-ray beam and enables fast and easy *in situ*

photon energy calibration. We also have checked the short-time reproducibility with fixed photon energy instead of NRS measurements. These information are described in Appendix A.

APPENDIX A Reproducibility with fixed photon energy

In this section, we describe stability and uniformity measurements with a fixed photon energy instead of NRS measurements. These measurements were done during beam time 3. The angles of both the HHM and the HRM were fixed, and the photon energy measurement was repeated for various mutual angles. As we described in the *Introduction*, the absolute photon energy can easily deviate because of changes in the thermal distribution of the monochromators. This cannot be avoided in the NRS measurement because the photon energy has to be scanned. The advantage of this study is that the monochromators can be fixed in the beamline. However, this measurement cannot distinguish between the fluctuation of the photon energy itself and that of the measurement system; therefore, it only indicates an upper bound in a short time range without an energy scan.

Fig. 11 shows the results of the repeated photon energy measurement, in which the photon energy was measured 23 times in ~ 85 min. The manual rotation table was fixed during the run. The peak-to-peak deviation was 17 meV. Fig. 12 shows the results of the measured energy for various mutual angles. The time required was 10–15 min for one point and

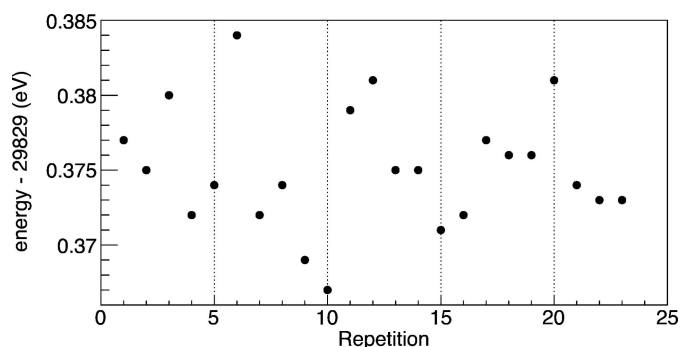


Figure 11
Repeated photon energy measurements.

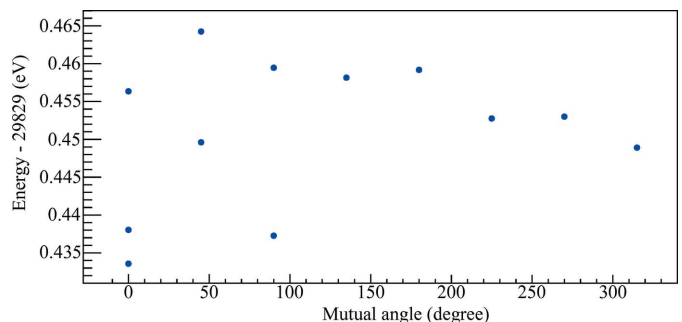


Figure 12
Photon energy measurements at various angle positions of SelfA.

~150 min for all points. The peak-to-peak deviation was 30 meV, which is smaller than the observed uncertainty described in the main text.

Acknowledgements

The synchrotron radiation experiments were performed on beamline BL19LXU at SPring-8 with the approval of the Japan Synchrotron Radiation Research Institute (JASRI) (proposals 2018A1326 and 2018B1436) and RIKEN (proposal Nos. 20180045 and 20190051). We thank all the staff at SPring-8, especially T. Kobayashi and K. Ishino, for building the operating software of the Bond diffractometer and for technical support for the experiment. We would like to thank Editage (<https://www.editage.com>) for English language editing.

Funding information

This work was supported by JSPS KAKENHI (grant No. JP18H01230 to Koji Yoshimura; grant No. JP19H00685 to Takahiko Masuda; grant No. JP19K14740 to Takahiro Hiraki; grant No. JP19K21879 to Akihiro Yoshimi). This project has received funding from the European Research Council (ERC) under the European Union's Horizon 2020 research and innovation programme (grant agreement No. 856415 'ThoriumNuclearClock' to Thorsten Schumm). Takahiko Masuda acknowledges the INAMORI Foundation for a grant.

References

- Arthur, J. (1989). *Rev. Sci. Instrum.* **60**, 2062–2063.
- Becker, P. & Stümpel, J. (1990). *Metrologia*, **27**, 127–132.
- Billinge, S. J. L. & Levin, I. (2007). *Science*, **316**, 561–565.
- Bond, W. L. (1960). *Acta Cryst.* **13**, 814–818.
- Burke, J. T. (2019). *Nature*, **573**, 202–203.
- Cavagnero, G., Fujimoto, H., Mana, G., Massa, E., Nakayama, K. & Zosi, G. (2004a). *Metrologia*, **41**, 445–446.
- Cavagnero, G., Fujimoto, H., Mana, G., Massa, E., Nakayama, K. & Zosi, G. (2004b). *Metrologia*, **41**, 56–64.
- Endt, P. M. (1990). *Nucl. Phys. A*, **521**, 1–400.
- Firestone, R. B. (1999). *Table of Isotopes*, 8th ed. Chichester: Wiley Interscience.
- Hall, J. (1967). *Phys. Rev.* **161**, 756–761.
- Herbstein, F. H. (2000). *Acta Cryst.* **B56**, 547–557.
- Hong, X., Chen, Z. & Duffy, T. (2012). *Rev. Sci. Instrum.* **83**, 063901.
- Kraft, S., Stümpel, J., Becker, P. & Kuetgens, U. (1996). *Rev. Sci. Instrum.* **67**, 681–687.
- Lyon, K. G., Salinger, G. L., Swenson, C. A. & White, G. K. (1977). *J. Appl. Phys.* **48**, 865–868.
- Masuda, T., Hiraki, T., Kaino, H., Kishimoto, S., Miyamoto, Y., Okai, K., Okubo, S., Ozaki, R., Sasao, N., Suzuki, K., Uetake, S., Yoshimi, A. & Yoshimura, K. (2019a). *Nucl. Instrum. Methods Phys. Res. A*, **913**, 72–77.
- Masuda, T. & Kajitani, M. (1993). *J. Rob. Mechatron.* **5**, 448–452.
- Masuda, T., Okubo, S., Hara, H., Hiraki, T., Kitao, S., Miyamoto, Y., Okai, K., Ozaki, R., Sasao, N., Seto, M., Uetake, S., Yamaguchi, A., Yoda, Y., Yoshimi, A. & Yoshimura, K. (2017). *Rev. Sci. Instrum.* **88**, 063105.
- Masuda, T., Yoshimi, A., Fujieda, A., Fujimoto, H., Haba, H., Hara, H., Hiraki, T., Kaino, H., Kasamatsu, Y., Kitao, S., Konashi, K., Miyamoto, Y., Okai, K., Okubo, S., Sasao, N., Seto, M., Schumm, T., Shigekawa, Y., Suzuki, K., Stellmer, S., Tamasaku, K., Uetake, S., Watanabe, M., Watanabe, T., Yasuda, Y., Yamaguchi, A., Yoda, Y., Yokokita, T., Yoshimura, M. & Yoshimura, K. (2019b). *Nature*, **573**, 238–242.
- Schmidbauer, M., Kwasniewski, A. & Schwarzkopf, J. (2012). *Acta Cryst.* **B68**, 8–14.
- Seiferle, B., von der Wense, L., Bilous, P., Amersdorffer, I., Lemell, C., Libisch, F., Stellmer, S., Schumm, T., Düllmann, C., Pálffy, A. & Thierolf, P. (2019). *Nature*, **573**, 243–246.
- Seto, M. (2012). *J. Phys. Soc. Jpn.* **82**, 021016.
- SPring-8 (2020). *SPring-8 operation modes*, http://www.spring8.or.jp/en/users/operation_status/schedule/bunch_mode. Accessed 23 January 2020.
- Thielking, J., Okhapikin, M., Głowacki, P., Meier, D., von der Wense, L., Seiferle, B., Düllmann, C., Thierolf, P. & Peik, E. (2018). *Nature*, **556**, 321–325.
- Watanabe, T., Fujimoto, H. & Masuda, T. (2005). *J. Phys. Conf. Ser.* **13**, 240–245.
- Watanabe, T., Kon, M., Nabeshima, N. & Taniguchi, K. (2014). *Meas. Sci. Technol.* **25**, 065002.
- Yabashi, M., Mochizuki, T., Yamazaki, H., Goto, S., Ohashi, H., Takeshita, K., Ohata, T., Matsushita, T., Tamasaku, K., Tanaka, Y. & Ishikawa, T. (2001). *Nucl. Instrum. Methods Phys. Res. A*, **467–468**, 678–681.
- Yamaguchi, A., Muramatsu, H., Hayashi, T., Yuasa, N., Nakamura, K., Takimoto, M., Haba, H., Konashi, K., Watanabe, M., Kikunaga, H., Maehata, K., Yamasaki, N. Y. & Mitsuda, K. (2019). *Phys. Rev. Lett.* **123**, 222501.
- Yoshimi, A., Hara, H., Hiraki, T., Kasamatsu, Y., Kitao, S., Kobayashi, Y., Konashi, K., Masuda, R., Masuda, T., Miyamoto, Y., Okai, K., Okubo, S., Ozaki, R., Sasao, N., Sato, O., Seto, M., Schumm, T., Shigekawa, Y., Stellmer, S., Suzuki, K., Uetake, S., Watanabe, M., Yamaguchi, A., Yasuda, Y., Yoda, Y., Yoshimura, K. & Yoshimura, M. (2018). *Phys. Rev. C* **97**, 024607.